Richtmyer-Meshkov instability in elastic-plastic media

A. R. Piriz* and J. J. López Cela
ETSI Industriales, Universidad de Castilla-La Mancha and Instituto de Investigaciones Energéticas, 13071 Ciudad Real, Spain

N. A. Tahir
Gesellschaft für Schwerionenforschung Darmstadt, Planckstrasse 1, 64291 Darmstadt, Germany

D. H. H. Hoffmann
Institut für Kernphysik, Technische Universität Darmstadt, 64289 Darmstadt, Germany

(Received 2 April 2008; published 5 November 2008)

An analytical model for the linear Richtmyer-Meshkov instability in solids under conditions of high-energy density is presented, in order to describe the evolution of small perturbations at the solid-vacuum interface. The model shows that plasticity determines the maximum perturbation amplitude and provides simple scaling laws for it as well as for the time when it is reached. After the maximum amplitude is reached, the interface remains oscillating with a period that is determined by the elastic shear modulus. Extensive two-dimensional simulations are presented that show excellent agreement with the analytical model. The results suggest the possibility to experimentally evaluate the yield strength of solids under dynamic conditions by using a Richtmyer-Meshkov-instability-based technique.

DOI: 10.1103/PhysRevE.78.056401 PACS number(s): 52.58.Hm, 52.50.Lp, 47.20.−k

I. INTRODUCTION

Hydrodynamic instabilities in solids under high-energy density conditions are governed by their elastic and plastic properties. At present the interest in this field is growing either because instabilities in solids are an object of research by itself or for their application as a tool for the experimental investigation of constitutive properties of matter [1–12]. In particular, Rayleigh-Taylor (RT) and Richtmyer-Meshkov (RM) instabilities may arise in the LAPLAS (Laboratory of Planetary Sciences) experiment proposed in the framework of the new FAIR (Facility for Antiproton and Ion Research) facility presently under construction at Gesellschaft für Schwerionenforschung (GSI) in Darmstadt [13,14]. This experiment is being designed for the study of equation of state and transport properties of high-energy density matter and consists in the quasi-isentropic implosion of a cylindrical shell driven by an intense heavy ion beam [15–17]. The ion beam with a ring shaped focal spot heats the annular region (the absorber) surrounding a shell that acts as a pusher. The pusher is made of a heavy metal and it is imploded by the absorber expansion thus compressing a material sample in the axial region. Hydrodynamic instabilities at the absorber-pusher interface could affect the implosion performance and, therefore, they must be investigated. Since the involved loading pressures are below the melting limit, the pusher remains in solid state during the implosion process. For this, we need to take into account the elastic-plastic constitutive properties of the shell material. The situation in the LAPLAS experiment is somewhat similar to the one present in magnetically accelerated shells [12,18], and in shells accelerated by gaseous detonation products [11,19,20].

On the other hand, RT instability has also been used as a tool for the experimental evaluation of the elastic limit of accelerated solids [4,10,11,19–22]. In fact, since the pioneering work by Barnes *et al.* [19,20], the use of RT instabilities in solids has been playing an increasing role in the experimental evaluation of material strength. This technique has been further developed in the last few years by introducing the laser driven quasi-isentropic acceleration of a plate with precut modulations. The acceleration is driven by pressures up to 200 GPa generated with high power laser facilities [4,10,11,21,22]. This recent progress allows, in principle, for achieving high loading pressures by keeping the sample below the melting temperature. Nevertheless, because of the relatively long pulse duration required by this technique, the maximum driving pressures obtained so far in the available laser facilities have been limited to values of around 200 GPa, postponing the achievement of the regime close to 1000 GPa up to the availability of the largest laser facility ever constructed, namely, the National Ignition Facility (NIF) in USA.

Probably because of the great interest in the RT based technique for the evaluation of yield strength, most of the work on hydrodynamic instabilities in matter under extreme conditions of pressure have concentrated on RT instability and relatively little effort has been dedicated to RM instability in solids with elastic-plastic constitutive properties [5,9,23]. RM instability occurs when a shock wave goes through an interface separating two media or when a shock is launched into a medium from an otherwise free surface, by the impact of a projectile on it [24–26]. Two recent studies, however, have analyzed the RM flow in perfectly elastic (Hookean) media and show that elasticity ensures the stability of the interface. As a result, the interface oscillates harmonically with a period that essentially depends on the solid shear modulus G [5,9]. For the more interesting and realistic case of elastic-plastic solids there exists, to our knowledge, only a study reported by Bakharakh *et al.* [23] consisting of numerical simulations. They found that after an initial time of monotonic growth, the perturbation amplitude reaches a

*roberto.piriz@uclm.es

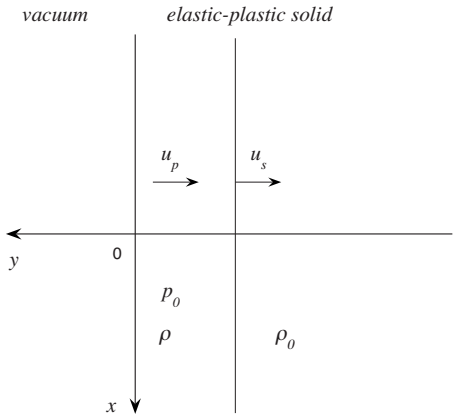

FIG. 1. Diagram of the solid-vacuum interface and of the shock wave separating the shocked region from the material unaffected by the shock

maximum and then remains close to it. From these numerical results they also found a scaling law for this maximum amplitude in terms of the yield strength Y and other material and experiment parameters. Nevertheless, this study was limited to relatively low driving pressures and hence, rather low compressions were obtained. More recently, Mikaelian [27] also presented a few results of numerical simulations. In addition, during the processing of this manuscript, the numerical simulations reported in Ref. [28] were noticed to us. However, no theoretical model has been proposed so far for the interpretation of numerical results.

In this paper we present an analytical model for the RM instability in solids that is constructed by assuming that the shocked material behaves similar to an elastic-perfectly plastic medium described by the Prandtl-Reuss flow rule with the von Mises yield criterion [29,30]. In addition, we have performed extensive two-dimensional (2D) numerical simulations with the finite element code ABAQUS [31] for comparison with the analytical results and we have found an excellent agreement between model and simulations. In the limit of relatively low shock compressions we retrieve the numerical results by Bakharakh *et al.* [23] both, with model and simulations.

II. THE ANALYTICAL MODEL

We consider a medium of density ρ with elastic-plastic properties that occupies the semi-space $y<0$ and has a free surface at $y=0$ (Fig. 1). We also assume that this interface has a small sinusoidal perturbation in the transverse direction of amplitude ξ_i and wavelength λ which are taken in such a way that $k\xi_i \ll 1$ ($k=2\pi/\lambda$ is the perturbation wave number). At $t=0$, a constant pressure p_0 is maintained at the solid-vacuum boundary ($y=0$), driving a shock which moves with constant velocity into the solid material. We concentrate here on the time asymptotic linear evolution of the interface corrugation that takes place once the shock traversed several wavelengths into the undisturbed material. We do not describe the details of the interaction between the shock and the interface during the transient phase in which the shock is still near $y=0$. As shown in Ref. [26], the effect of such an interaction would be to generate a rotational velocity field inside the shock compressed material. This rotational velocity field has characteristic lengths that cannot be determined self-consistently from the present model. We also assume that the perturbations are incompressible.

As we have previously discussed in Ref. [5], the asymptotic evolution of the interface, that is, after an initial transient phase, can be described by considering that the only force acting on the interface is the one due to the shear stress. The shear stress is described by the deviatoric part S_{ij} of the stress tensor $\sigma_{ij}=-p\delta_{ij}+S_{ij}$, where p is the thermodynamic pressure (the isotropic part of σ_{ij}) and δ_{ij} is the identity tensor. In addition, as we have shown in Refs. [5,8,32], an approximate equation of motion can be derived by assuming a perturbed velocity field of the following form:

$$v_y = \dot{\xi}(t)e^{qy}\sin kx, \tag{1}$$

$$v_x = \dot{\zeta}(t)e^{q_x y}\cos kx, \tag{2}$$

where $\dot{\xi}(t)$ is the instantaneous normal velocity of the interface and q^{-1} and q_x^{-1} are the characteristic lengths with which the surface modes decay with distance from the interface. As we have discussed above, q and q_x must be imposed into the model equations in the same manner it has been done in the past in similar models for the RT instability problem [6–8,33–37] and for the RM flow problem in purely elastic media [5]. Thus, we take $q^{-1}=\alpha k^{-1}$ and $q_x^{-1}=\alpha_x k^{-1}$, where α is a numerical factor that express our ignorance about the exact velocity field and that will be obtained by comparison with the numerical simulation results. Incompressibility of the perturbations ($\partial v_i/\partial x_i=0$) requires that $q\dot{\xi}=k\dot{\zeta}$ at $y=0$. On the other hand, $\alpha_x=k/q_x$ will be determined, as we will see later, from the self-consistency of the equation of motion.

With the previous assumptions we can write the equation of motion for the asymptotic linear evolution of the interface [5–8]:

$$\rho\frac{\alpha}{k}\frac{dv_y}{dt} = -S_{yy} \tag{3}$$

(see Ref. [5] for more details about derivation of this equation) where now S_{yy} is the perturbation of the normal component of the deviatoric part of the stress tensor. Hereafter, S_{ij} will denote the perturbation of the deviatoric part of the stress tensor. In addition, ρ is the post-shock density and it is determined by the pressure p_0 driving the shock and by the equation of state (EOS) of the solid material. Here, as in Refs. [23,30], we have adopted a Mie-Grüneisen EOS with a Grüneisen coefficient $\Gamma=\rho_0\Gamma_0/\rho$ (Γ_0 is a material parameter). In addition, in order to express the Hugoniot of the solid we have taken the usual linear relationship between the shock velocity u_s and the particle velocity u_p:

$$p - p_h = \rho_0\Gamma_0(\epsilon - \epsilon_h) \tag{4}$$

$$u_s = c_0 + su_p, \tag{5}$$

where p and ϵ are the pressure and the specific internal energy of the material, and the index "h" denotes the Hugoniot

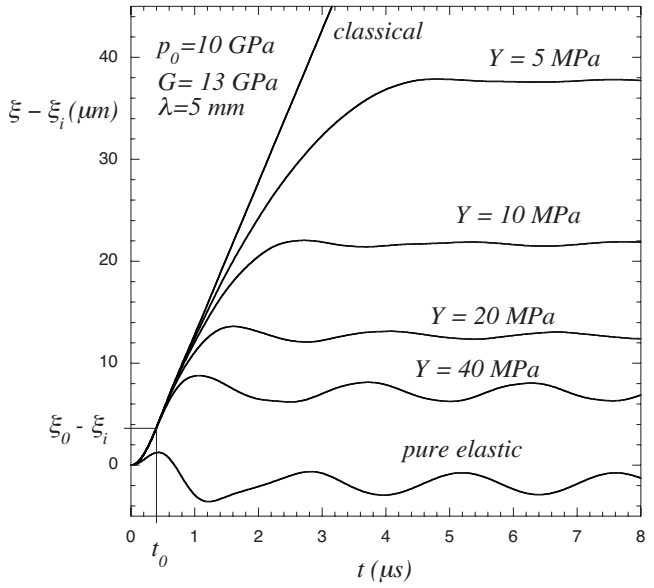

FIG. 2. Relative perturbation amplitude as a function of time for different values of the yield strength Y. Perturbation growth for an ideal fluid (classical) and for a pure elastic medium are also shown.

reference state. The constants c_0 and s are parameters characteristic of the material. Therefore, the following relationships between the post-shock density ρ and the driving pressure p_0 can be written as

$$\eta = 1 - \frac{\rho_0}{\rho}, \quad p_0 - p_i = \frac{\rho_0 c_0^2 \eta}{(1 - s\eta)^2}, \quad u_p = \frac{c_0 \eta}{1 - s\eta}, \tag{6}$$

where p_i is the initial pressure of the material (usually it is $p_i \ll p_0$). Then, Eq. (3) can be used to describe the interface evolution after an initial transient phase. Two-dimensional (2D) numerical simulations show that during this transient phase the material does not feel the effect of the constitutive properties and, thus, it evolves similar to the classical case for an ideal fluid ($S_{ij}=0$) (Fig. 2). We will further discuss this point later. Now, in order to describe the interface evolution after such an initial transient phase, we need to derive a suitable expression for the normal component S_{yy} of the deviatoric part of the stress tensor. In Ref. [8] we have obtained S_{yy} for viscous fluids and elastic (Hookean) solids. Here we have to find S_{yy} for an elastic-plastic material.

A. Elastic-plastic media

In order to get a convenient expression for the tensor S_{ij} we assume a Prandtl-Reuss rule with the von Mises yield stress criterion [29]

$$\dot{S}_{ij} + 2GS_{ij}\frac{S_{mn}D_{mn}}{S_{mn}S_{mn}} = 2GD_{ij} \tag{7}$$

if

$$S_{ij}D_{ij} > 0 \quad \text{and } S_{ij}S_{ij} = \frac{2}{3}Y^2 \tag{8}$$

and

$$\dot{S}_{ij} = 2GD_{ij} \tag{9}$$

if

$$S_{ij}D_{ij} < 0 \quad \text{or } S_{ij}S_{ij} < \frac{2}{3}Y^2, \tag{10}$$

where, by assuming that perturbations are incompressible ($\partial v_i/\partial x_i = 0$), we have

$$D_{ij} = \frac{1}{2}\left(\frac{\partial v_i}{\partial x_j} + \frac{\partial v_j}{\partial x_i}\right). \tag{11}$$

Following Ref. [29], for convenience, we define the time independent tensor M_{ij} as follows:

$$M_{ij} = \frac{D_{ij}}{k\dot{\xi}}. \tag{12}$$

In the previous equations we have used usual index notation in which repeated indices denote summation. Then, multiplying Eq. (7) by D_{ij} and defining suitable dimensionless variables, we get a differential equation for the product $S_{ij}M_{ij}$ [29]:

$$\frac{d\Phi}{d\bar{x}} + \Phi^2 = 1, \quad \Phi(\bar{x}_0) = \Phi_0, \tag{13}$$

where

$$\Phi = \frac{S_{ij}M_{ij}}{|M|\sqrt{\frac{2}{3}Y}}, \quad \bar{x} = \frac{2kG|M|}{\sqrt{\frac{2}{3}Y}}\xi, \quad |M|^2 = M_{ij}M_{ij}. \tag{14}$$

For deriving Eq. (13) we have used the following relationships:

$$\dot{S}_{ij}M_{ij} = \frac{\partial(S_{ij}M_{ij})}{\partial t} = \dot{\xi}\frac{\partial(S_{ij}M_{ij})}{\partial \xi}, \tag{15}$$

where M_{ij} is independent of time and $\dot{\xi} = d\xi(t)/dt$.

The solution of Eq. (13) turns out to be [29]

$$\Phi(\bar{x}) = \frac{\Phi_0 + \tanh(\bar{x} - \bar{x}_0)}{1 + \Phi_0 \tanh(\bar{x} - \bar{x}_0)}. \tag{16}$$

Introducing this result into Eq. (7) we get the differential equations for the components of the tensor S_{ij}:

$$\frac{dS}{d\bar{x}} + \Phi(\bar{x})S = 1, \quad S(\bar{x}_0) = S_0, \tag{17}$$

where we have defined S as

$$S = \frac{|M|}{\sqrt{\frac{2}{3}}YM_{ij}}S_{ij}. \tag{18}$$

By solving Eq. (17) we get

$$S = \frac{S_0 + \tanh(\bar{x} - \bar{x}_0)}{1 + S_0 \tanh(\bar{x} - \bar{x}_0)}. \quad (19)$$

Since we are considering the regime for which, at $\bar{x}=\bar{x}_0$, the material is already on the yield surface, it results to be $S_0=1$ and therefore, $S=1$ for all values of $\bar{x}$ (provided that $S_{ij}D_{ij}>0$ and $|S|=\sqrt{2/3}Y$). Thus, the deviatoric tensor S_{ij} is

$$S_{ij} = \sqrt{\frac{2}{3}}\frac{M_{ij}}{|M|}Y, S_{ij}D_{ij} > 0 (k\dot{\xi} > 0), \quad |S|^2 = \frac{2}{3}Y^2. \quad (20)$$

On the other hand, when $S_{ij}D_{ij}<0$ $(k\dot{\xi}<0)$ or $|S|<\sqrt{2/3}Y$, we have to use Eq. (9). Then, by proceeding in the same manner used to obtain Eq. (13), we get

$$\frac{\partial(S_{ij}M_{ij})}{\partial\xi} = 2kG|M|^2. \quad (21)$$

Upon integration the previous equation yields

$$S_{ij} = 2kGM_{ij}(\xi - \bar{\xi}), k\dot{\xi} < 0 \quad \text{or} \quad |S| < \sqrt{\frac{2}{3}}Y, \quad (22)$$

where $\bar{\xi}$ represents the amplitude mean values around which elastic oscillations take place during the elastic phases.

B. Model results

Equations (20) and (22) provide the required expression of S_{yy} that we must introduce into the equation of motion. However, in order to use these equations the perturbed velocity field must be specified. As we have already mentioned, we will adopt the expressions given by Eqs. (1) and (2) with $q^{-1}=\alpha k^{-1}$ and $\dot{\zeta}=\dot{\xi}/\alpha$. Instead, for determining α_x in terms of α, we notice that consistency of Eq. (3) demands that $|M|$ must be independent of the coordinate x. Therefore, at $y=0$, we have

$$|M|^2 = \frac{2}{\alpha^2} = \frac{1}{2}\left(\frac{1}{\alpha\alpha_x} + 1\right)^2. \quad (23)$$

The previous equation provide $\alpha_x(\alpha)$ and so, q_x can be evaluated after the parameter α is specified. Also we obtain

$$M_{yy} = \frac{\sin kx}{\alpha}. \quad (24)$$

By defining $S_y=S_{yy}/\sin kx$ and using Eq. (24), the equation of motion of the interface $(y=0)$ reads

$$\rho\frac{\alpha}{k}\ddot{\xi} = -S_y, \quad (25)$$

where:

$$S_y = \begin{cases} \sqrt{\frac{2}{3}}\frac{Y}{\alpha|M|}, & k\dot{\xi} > 0, \xi \geq \xi_p, \\ 2\frac{k}{\alpha}G(\xi - \bar{\xi}), & k\dot{\xi} < 0, \xi \leq \xi_p, \end{cases} \quad (26)$$

where $\xi_p-\xi_i$ is the amplitude for which the elastic limit is achieved (ξ_i is the initial amplitude when the material is stress-free and, therefore, for the initial elastic phase it is $\bar{\xi}=\xi_i$):

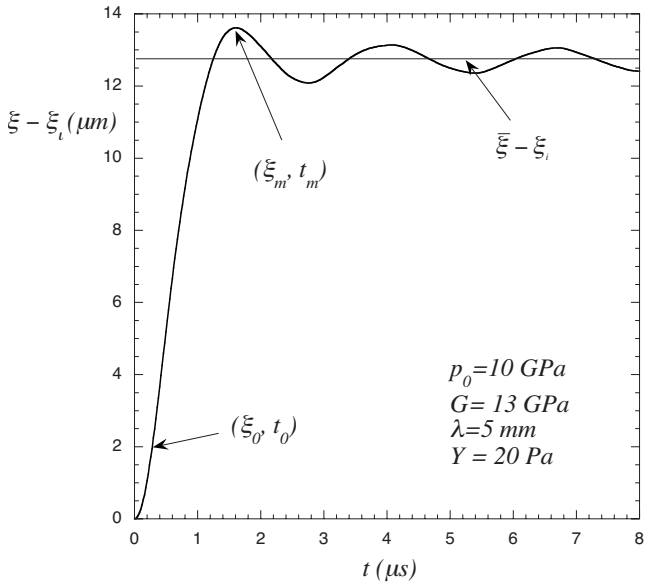

FIG. 3. Relative perturbation amplitude as a function of time for a typical case. Amplitude and frequency vary during the first oscillation period of the elastic phase.

$$\xi_p - \xi_i = \sqrt{\frac{2}{3}}\frac{1}{2|M|}\frac{Y}{kG}. \quad (27)$$

As we have already mentioned, there is an initial transient phase during which the material seemingly does not feel the effects of the constitutive properties on the interface evolution and, thus, the perturbations grow as in the classical case for an ideal fluid (see Fig. 2) [5]. After this transient phase (for times $t \geq t_0$), when the perturbation amplitude $\xi(t)$ has growth up to a value $\xi_0 > \xi_i$ $[\xi_0=\xi(t_0)]$, Eqs. (25) and (26) can be used for describing the interface evolution. For most cases of practical interest we can assume that at $t=t_0$, the amplitude has already overcome the elastic limit $(\xi_0 \geq \xi_p)$ and thus

$$\xi_0 - \xi_i \geq \sqrt{\frac{2}{3}}\frac{1}{2|M|}\frac{Y}{kG}. \quad (28)$$

Therefore, the later evolution will take place within the plastic regime $(\xi \geq \xi_p)$, provided that $k\dot{\xi}>0$. Actually, as we will see later, this assumption is not very restrictive because in every case the amplitude will grow up to a maximum value ξ_m that will be reached at the time t_m and, for times $t \geq t_m$, the material will remain always into the purely elastic regime (Fig. 3). So, by taking $\xi_p \leq \xi_0$, we neglect only an intermediate regime for which it is $\xi_0 \leq \xi_p \leq \xi_m$ and a short elastic phase exists after the initial transient phase. In any case such an intermediate regime can also be described by the present model. Here we restrict ourselves to the most interesting regime defined by Eq. (28).

By integrating Eqs. (25) and (26) for times $t \leq t_m$, we get

$$\dot{\xi} - \dot{\xi}_0 = -\sqrt{\frac{2}{3}}\frac{1}{\alpha^2|M|}\frac{kY}{\rho}(t - t_0), \tag{29}$$

$$\xi - \xi_0 = \dot{\xi}_0(t - t_0) - \sqrt{\frac{2}{3}}\frac{1}{2\alpha^2|M|}\frac{kY}{\rho}(t - t_0)^2. \tag{30}$$

Then, the maximum amplitude ξ_m and the time t_m when this maximum is reached are given by the following equations:

$$\xi_m - \xi_0 = \sqrt{\frac{3}{2}}\frac{\alpha^2|M|}{2}\frac{\rho\dot{\xi}_0^2}{kY}. \tag{31}$$

$$t_m - t_0 = \sqrt{\frac{3}{2}}\alpha^2|M|\frac{\rho\dot{\xi}_0}{kY}. \tag{32}$$

For times $t \leqslant t_0$ the amplitude grows classically (like in an ideal fluid) and it reaches the asymptotic velocity that will be the initial velocity $\dot{\xi}_0$ for the following plastic phase. Therefore, we have [24–26]:

$$\dot{\xi}_0 = k\xi_i u_p, \tag{33}$$

where u_p, as well as ρ in the previous equations, are determined by the driving pressure p_0 and the material constants [see Eqs. (6)]. By introducing Eqs. (6) with $p_i \ll p_0$ into Eq. (33) and then replacing it into Eq. (31), we get after a short algebra:

$$\frac{\xi_m - \xi_0}{\xi_0} \approx \sqrt{\frac{3}{2}}\frac{\alpha^2|M|}{2}\frac{k\xi_0 p_0^2}{Y\rho_0 c_0^2}\left(\frac{\xi_i}{\xi_0}\right)^2\frac{(1 - s\eta)^2}{1 - \eta}. \tag{34}$$

In the limit of relatively low yield strength Y ($Y/k\xi_0 G \ll 1$) it results to be $\xi_0 \approx \xi_i$, and for weak shock compressions it is $\eta \ll 1$. Therefore, the previous equation reads

$$\frac{\xi_m - \xi_i}{\xi_i} \approx \sqrt{\frac{3}{2}}\frac{\alpha^2|M|}{2}\frac{k\xi_i p_0^2}{Y\rho_0 c_0^2}. \tag{35}$$

This expression reproduces exactly the scaling law found by Bakharakh *et al.* [23] from a series of 2D numerical simulations. As we will see later, the numerical simulations can be very well fitted by taking $\alpha = 0.335$ ($|M| = 4.223$) so that the constant in Eq. (34) is $\sqrt{3/2}(\alpha^2|M|/2) \approx 0.29$.

For times $t \geqslant t_m$ it is $\dot{\xi} \leqslant 0$ and the material enters in the elastic regime described by the second branch of Eq. (26). In such a case, the equation of motion reads [5]:

$$\rho\frac{\alpha}{k}\ddot{\xi} = -2\frac{k}{\alpha}G(\xi - \bar{\xi}). \tag{36}$$

However, the numerical simulations show that the transition from the plastic to the elastic regimes does not happen instantaneously at $t = t_m$ but instead, it requires a time of the order of one oscillation period during which the perturbed velocity field varies and adjusts to the new elastic regime. Of course, the description of such a transition time is out of the scope of our model but, nevertheless, the essential features of the transition effects can be captured with the parameter α. In fact, during this transient period the value of our parameter changes from $\alpha = 0.335$ in the plastic regime, up to its final value $\alpha = \alpha_e = 1.55$ [5] in the later elastic phase. This transition can be observed in the typical case shown in Fig. 3 (for times $t \geqslant t_m$) as a variation in both, the oscillation amplitude and frequency during a time of the order of one oscillation period. After that time the interface remains oscillating harmonically with a practically constant amplitude and frequency as described by Eq. (36).

Since the initial conditions for this oscillating elastic phase are settled by the precedent plastic phase, we can obtain the mean value $\bar{\xi}$ around which the elastic oscillations take place asymptotically:

$$\xi_m - \bar{\xi} = \sqrt{\frac{2}{3}}\frac{1}{2|M|}\frac{Y}{kG}, \tag{37}$$

where $|M|$ is calculated from Eq. (23) ($\alpha_e = 1.55$, $|M| = 0.91$, $\sqrt{2/3}/2|M| \approx 0.45$).

In a similar manner, we can get the oscillation period in the asymptotic elastic regime from Eq. (36) [5,9]:

$$T = \alpha_e \lambda\sqrt{\frac{\rho}{2G}}. \tag{38}$$

III. COMPARISON WITH 2D NUMERICAL SIMULATIONS

In order to complete our study we have performed extensive 2D numerical simulations using the explicit version of the ABAQUS code. This code is based on the finite element method and assumes a Lagrangian representation. The time integration of the dynamic equilibrium equations is achieved via a central difference scheme, that is an explicit second-order accuracy algorithm and conditionally stable. To provide the computational efficiency associated with the explicit dynamic procedure, diagonal element mass matrices are used. The spatial discretization is performed by means of four-node bilinear elements with reduced integration and hourglass control.

For the numerical calculations we have taken a plate that has periodic symmetry boundaries at the edges, so that, a plate in plane strain of infinite lateral extent is modeled. Besides, we consider that it has a thickness d, which is large compared with the perturbation wavelength ($kd \gg 1$), so that, the plate can be considered as a semispace. We have considered two different perturbation wavelengths $\lambda = 5$ and $\lambda = 10$ mm with 80 elements per wavelength and we have taken a fixed initial amplitude $\xi_i = 20$ μm. Moreover, for the Mie-Grüneisen EOS we have taken the following parameter values: $\Gamma_0 = 2.16$, $s = 1.337$, $c_0 = 5380$ m/s, and $\rho_0 = 2.7$ g/cm^3. Actually, these values correspond to an aluminum sample but here we have taken them just as a reference case without intending the consideration of any particular material.

On the other hand, we have assumed an elastic-perfectly plastic model for the material. Of course, this model may not be realistic but, however, it is more appropriate to elucidate the effects of the various parameters. Therefore, the parameters of the constitutive model (namely, G and Y) have been varied in order to consider the whole range of possible re-

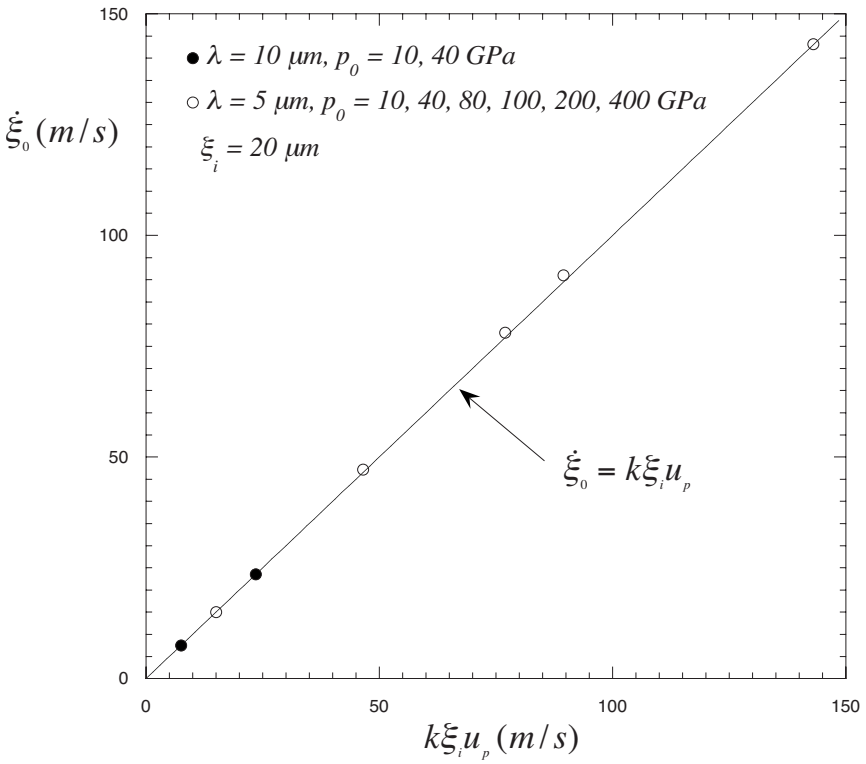

FIG. 4. Comparison between the initial velocity $\dot{\xi}_0$ with the classical asymptotic value $k\xi_i u_p$. Dots are obtained from the numerical simulations.

gimes even if they may not correspond to realistic values for Al parameters. Besides, we have taken different values of the constant pressure that launches the shock into the plate: $p_0 = 10, 40, 80, 100, 200, 400$ GPa. For the highest pressures, we get considerable compression factors ($\eta \sim 0.5$), extending in this way the range of parameters explored in Ref. [23] and allowing us to check the more general scaling law given by Eq. (31). As we have already shown, the scaling obtained by Bakharakh *et al.* [23] and given by Eq. (35) is a particular case of Eq. (31).

We have also considered several values of the shear modulus $G=3$, 13, 26, and 80 GPa. Then, the yield strength Y was varied taking into account that condition given by Eq. (28) was satisfied, in such a way that the perturbation evolves into the plastic regime immediately after the end of the initial transient phase (that is, during the time interval $t_0 \leqslant t \leqslant t_m$).

From the numerical simulations we have evaluated the time t_0 and the amplitude ξ_0 when the effects of the plastic constitutive properties start to be felt. For this, we have taken into account that for $t \leqslant t_0$ the perturbation grows classically and then, it must be $\ddot{\xi} \geqslant 0$ and that for $t \geqslant t_0$, the perturbation grows in the plastic regime and then, it must be $\ddot{\xi} \leqslant 0$ [see Eq. (25)]. Therefore, the amplitude ξ_0 is taken at the inflection point [$\ddot{\xi}(t_0)=0$]. At this time ($t=t_0$) we assume that the asymptotic classical velocity $\dot{\xi}_0$ has been already reached and so, it is given by Eq. (33). We have checked this assumption by comparing in Fig. 4 the value of $\dot{\xi}_0$ given by the numerical simulations with the result yielded by Eq. (33) where we can see that an excellent agreement exists.

On the other hand, in Figs. 5 and 6, respectively, we compare the maximum amplitude ξ_m and the instant t_m evaluated from the numerical simulations, with Eqs. (31) and (32), for many different cases as indicated in the figures. We see that, in order to fit the numerical calculations we can take $\alpha = 0.335$ and thus, we have

$$\xi_m - \xi_0 \approx 0.29 \frac{\rho \dot{\xi}_0^2}{kY}, \tag{39}$$

$$t_m - t_0 \approx 0.58 \frac{\rho \dot{\xi}_0}{kY}. \tag{40}$$

Once the perturbation enters in the asymptotic elastic regime, we have a constant oscillation period that can be evaluated from the numerical simulations. The simulation data are shown in Fig. 7 together with the values given by Eq. (38) with $\alpha_e = 1.55$ [5].

In this regime we can also evaluate the asymptotic mean value $\bar{\xi}$ around which the elastic oscillations occur. As we can see in Fig. 8, within the limits imposed by Eq. (28), these data are well fitted by Eq. (37) with a numerical coefficient $\sqrt{2/3}/2|M| \approx 0.68$ which differs the value obtained with $\alpha_e = 1.55$ by 50%: $\sqrt{2/3}/2|M| \approx 0.45$ [by choosing a larger value $\alpha_e = 1.9$ the numerical factors in Eqs. (37) and (38) differ less than 24% from the simulation results]. Beyond such a limit, the transition to the plastic regime occurs at a time t_p ($t_0 \leqslant t_p \leqslant t_m$) and as t_p approaches to t_0, the transition does not happens and then, the material remains into the purely elastic regime [5,9].

It may be worth to notice that in many cases of practical interest, the amplitude of the elastic oscillations is much smaller than the maximum perturbation amplitude ξ_m ($\xi_m - \bar{\xi} \ll \xi_m - \xi_0$) and, therefore, it is $\xi_m \approx \bar{\xi}$:

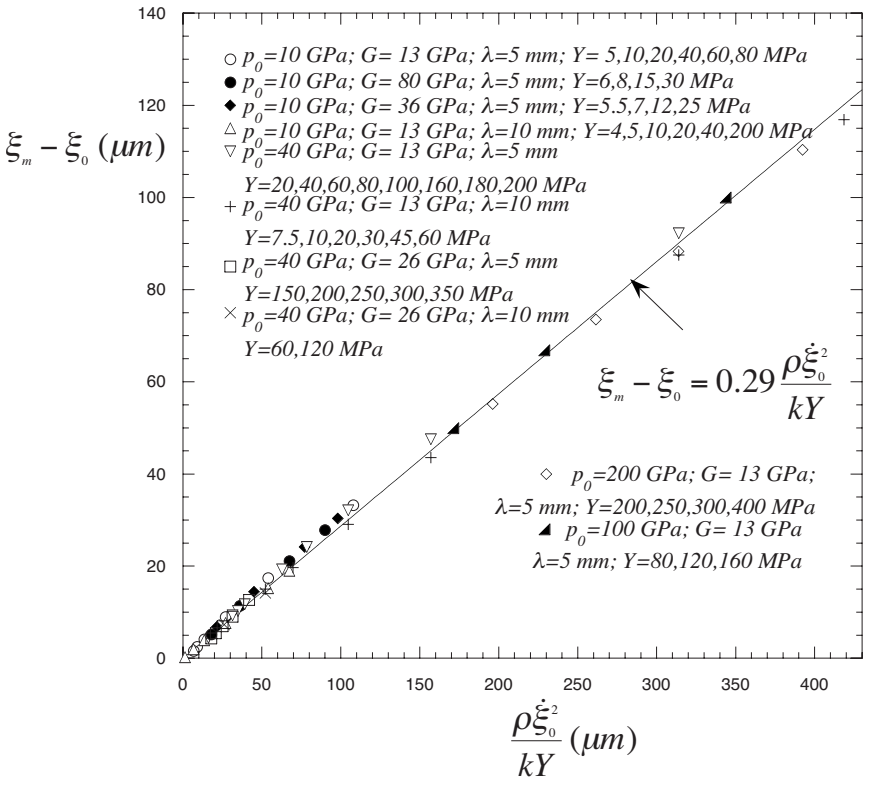

FIG. 5. Maximum relative amplitude as a function of the parameters combination $\rho\dot{\xi}_0^2/kY$. Dots are obtained from the numerical simulations.

$$\bar{\xi} - \xi_0 \approx 0.29\frac{\rho\dot{\xi}_0^2}{kY}. \tag{41}$$

Such a mean value of the amplitude can be used to measure the yield strength Y. At present the technique of induced RT instability is currently used to experimentally evaluate the material strength at high pressure [4,10,11]. In principle, this technique allows for reaching driving pressures of the order of 1000 GPa, provided that this pressure is applied gently enough to avoid strong shocks and melting of the sample. However, such a high level of loading could only be reached in future on the biggest facilities as, for instance, the

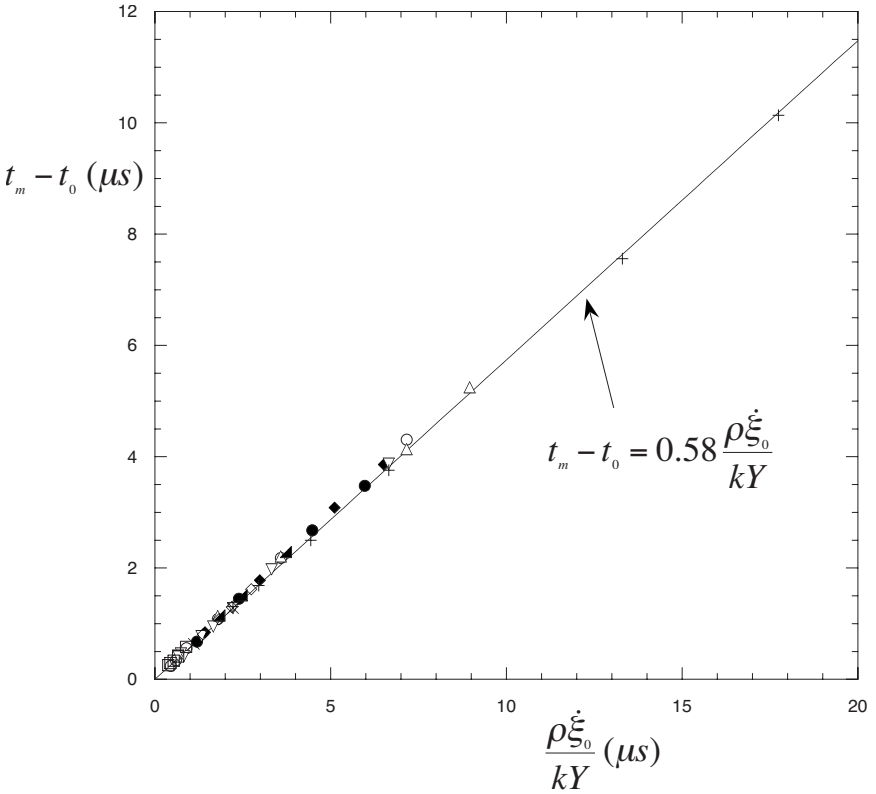

FIG. 6. Relative time at which maximum amplitude is achieved as a function of the parameters combination $\rho\dot{\xi}_0/kY$. Dots correspond to the same cases as indicated in Fig. 5.

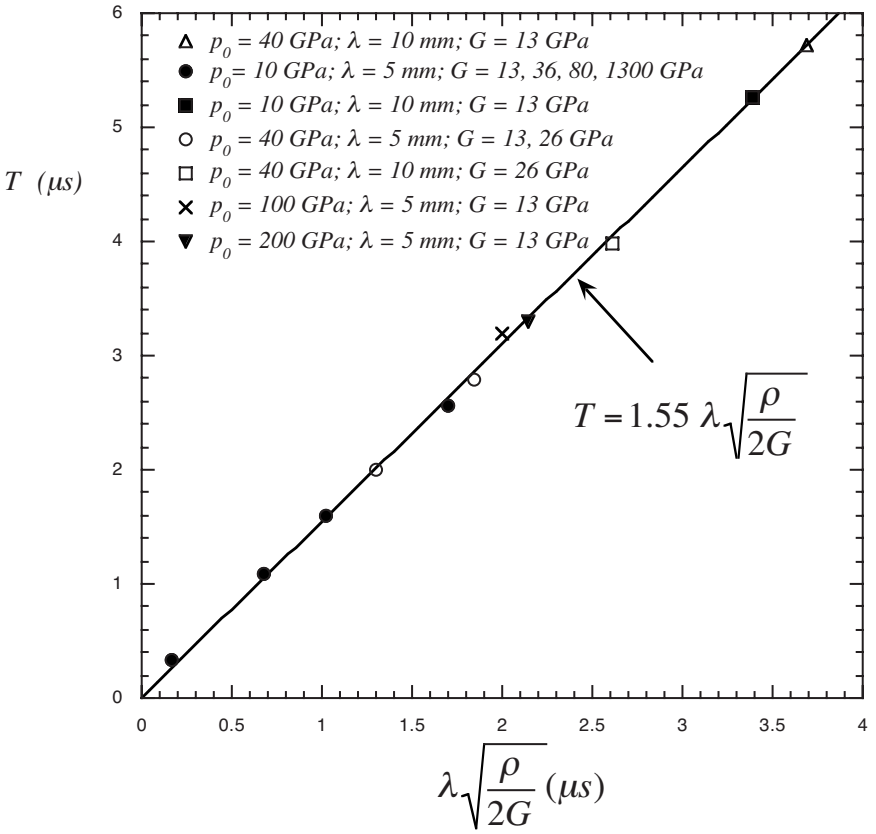

FIG. 7. Oscillation period in the asymptotic elastic regime. Dots are obtained from the numerical simulations.

NIF laser [4,10,11], but so far it has been limited to driving pressures of the order of 200 GPa in Al. At the level of $p_0 \leqslant 100$ GPa in Al a single shock can be used without reaching the melting point [10,38]. This is a very interesting regime that is being currently explored with the RT instability technique but that could be studied alternatively by using a RM based technique. Instead to measure the growth rate of RT induced instability, Eq. (41) suggests that a unique measurement of the perturbation amplitude can give an experimental evaluation of the yield strength Y, provided that it is taken at

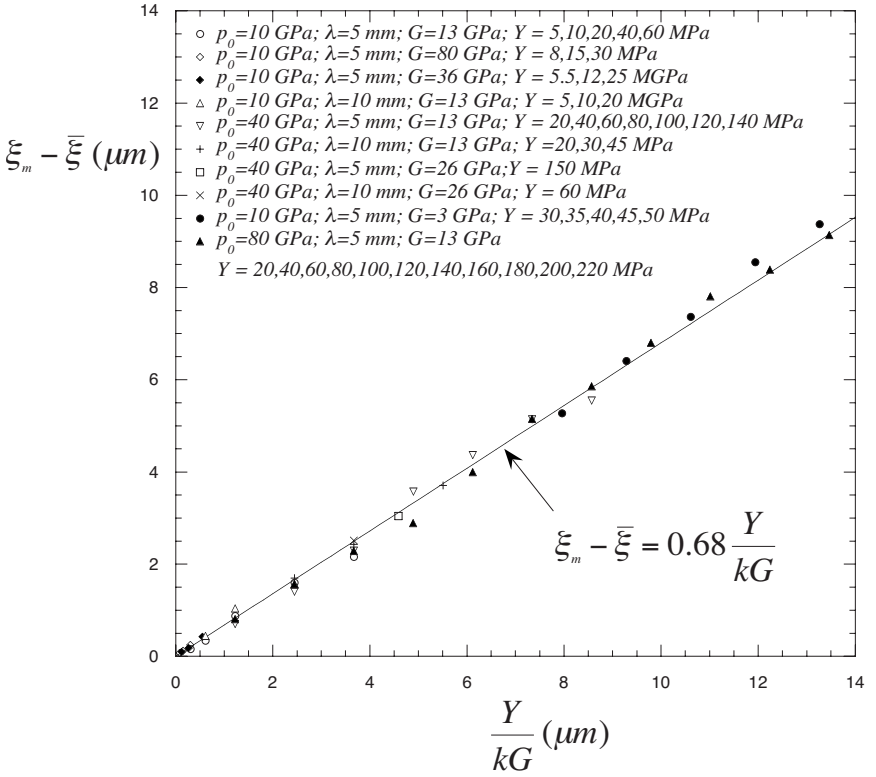

FIG. 8. Relative mean value of the maximum amplitude $\xi_m - \bar{\xi}$ as a function of the parameters combination Y/kG. Dots are the result of numerical simulations.

relatively long times $t \geqslant t_m$, once the material has reached the elastic regime. This RM based technique may be easier to implement than the presently used RT technique which requires more measurements at different instants and it can take advantage of relatively modest facilities more easily available. In addition, since yield strength depends also on the temperature and of the strain rate (for stresses below 10 GPa) [38], it can allow us to explore the complementary region of relatively higher temperatures. Thus, RT and RM based techniques will determine the yield strength at different regimes allowing for the better validation of existing strength models.

IV. CONCLUDING REMARKS

We have used the relatively simple method presented in Refs. [5,8] for developing an analytical model for the RM instability of solids under extreme conditions of pressure. The model yields simple formulas with character of scaling laws for describing some essential features that are characteristic of the instability perturbation growth in solids with elastic-plastic constitutive properties. In agreement with a previous numerical study, the model shows that as a consequence of the shock interaction with the interface, the initial perturbations grow up to a maximum amplitude that depends on the yield strength of the medium. Then, the material enters into a purely elastic regime and, after a transition time, it remains oscillating with a constant amplitude and frequency.

We have performed a set of 2D numerical simulations that agree very well with the analytical scaling laws and they allow us to determine the numerical coefficients that the model cannot yield because they are related to the actual velocity field. Thus, we have presented an analytical model that provides a physical picture of the RM instability in solids and that, with the fitting coefficients α and α_e, it also gives rather good quantitative results. Of course, a perfect agreement between model and simulation cannot be expected essentially because of the nature of the model approximations. In fact, the ignorance of the real perturbed velocity field (which we have to impose instead to obtain it in a self-consistent manner) has been packed in the parameters α and α_e. A self-consistent treatment similar to the one presented in Ref. [26] for ideal gases would be necessary for nonideal media. Such a treatment has not been performed so far. Nevertheless, the features of the present model make it very suitable for the conceptual design of new experiments. In particular, our results suggest the possibility to explore an alternative regime of the constitutive properties of solids by using a RM instability based technique instead of the one currently used based on the RT instability. This can allow for reaching similar levels of the driving pressures ($\leqslant$100 GPa for Al in order to prevent melting) and relatively higher temperatures. However, since pressure can be directly driven without the requirement of a previous step of pressurizing a reservoir [4,10,39], more modest facilities could be used.

ACKNOWLEDGMENTS

The authors wish to thank to G. Wouchuk for very helpful discussions. This work has been partially supported by the Ministerio de Ciencia y Tecnología (Grants No. FIS2006-05389, No. DPI2005-02278) and by the Consejería de Ciencia y Tecnología of Spain (Grant No. PAI-0152-7994) and by the BMBF of Germany, and it has been performed under the International Atomic Energy (IAEA) Agreement No. 13820/R0.

[1] A. L. Mikhailov, Phys. Mesomech. **10**, 265 (2007).
[2] G. Terrones, J. Appl. Phys. **102**, 034908 (2007).
[3] G. Terrones, Phys. Rev. E **71**, 036306 (2005).
[4] B. A. Remington, P. Allen, E. M. Bringa, J. Hawreliak, D. Ho, K. T. Lorenz, H. Lorenzana, J. M. McNaney, M. A. Meyers, S. W. Pollaine, K. Rosolankova, B. Sadik, M. S. Schneider, D. Swift, J. Wark, and B. Yaakobi, J. Mater. Sci. Technol. **22**, 474 (2006).
[5] A. R. Piriz, J. J. Lopez Cela, N. A. Tahir, and D. H. H. Hoffmann, Phys. Rev. E **74**, 037301 (2006).
[6] A. R. Piriz, J. J. Lopez Cela, M. C. Serna Moreno, N. A. Tahir, and D. H. H. Hoffmann, Laser Part. Beams **24**, 275 (2006).
[7] J. J. Lopez Cela, A. R. Piriz, M. C. Serna Moreno, and N. A. Tahir, Laser Part. Beams **24**, 427 (2006).
[8] A. R. Piriz, J. J. Lopez Cela, O. D. Cortazar, N. A. Tahir, and D. H. H. Hoffmann, Phys. Rev. E **72**, 056313 (2005).
[9] J. N. Plohr and B. J. Plohr, J. Fluid Mech. **537**, 55 (2005).
[10] K. T. Lorenz, M. J. Edwards, S. G. Glendinning, A. F. Jankowsky, J. McNaney, S. M. Pollaine, and B. A. Remington, Phys. Plasmas **12**, 056309 (2005).
[11] J. D. Colvin, M. Legrand, B. A. Remington, G. Shurtz, and S. V. Weber, J. Appl. Phys. **93**, 5287 (2003).
[12] R. E. Reinovsky, W. E. Anderson, W. L. Atchison, C. E. Ekdahl, R. J. Faehl, I. R. Lindemuth, D. V. Morgan, M. Murillo, J. L. Stokes, and J. S. Shlachter, IEEE Trans. Plasma Sci. **30**, 1764 (2002).
[13] W. F. Henning, Nucl. Instrum. Methods Phys. Res. B **214**, 211 (2004).
[14] N. A. Tahir, A. Adonin, C. Deutsch, V. E. Fortov, N. Grandlouan, B. Geif, V. Gayaznov, D. H. H. Hoffmann, M. Kulish, I. V. Lomonosov, V. Mintsev, P. Ni, D. Nikolaev, A. R. Piriz, N. Shilkin, P. Spiller, A. Shutov, M. Temporal, V. Ternovoi, S. Udrea, and D. Varentsov, Nucl. Instrum. Methods Phys. Res. A **544**, 16 (2005).
[15] N. A. Tahir, D. H. H. Hoffmann, A. Kozyreva, A. Tauschwitz, A. Shutov, J. A. Maruhn, P. Spiller, U. Neuner, J. Jacoby, M. Roth, H. Juranek, and R. Redmer, Phys. Rev. E **63**, 016402 (2001).
[16] N. A. Tahir, H. Juranek, A. Shutov, R. Redmer, A. R. Piriz, M. Temporal, D. Varentsov, S. Udrea, D. H. H. Hoffmann, C. Deutsch, I. Lomonosov, and V. E. Fortov, Phys. Rev. B **67**, 184101 (2003).
[17] A. R. Piriz, R. F. Portugues, N. A. Tahir, and D. H. H. Hoffmann, Phys. Rev. E **66**, 056403 (2002).

[18] R. K. Keinigs, W. L. Atchison, R. J. Faehl, V. A. Thomas, K. D. McLenithan, and R. J. Trainor, J. Appl. Phys. **85**, 7626 (1999).
[19] J. F. Barnes, P. J. Blewet, R. G. McQueen, K. A. Meyer, and D. Venable, J. Appl. Phys. **45**, 727 (1974).
[20] J. F. Barnes, D. H. Janney, R. K. London, K. A. Meyer, and D. H. Sharp, J. Appl. Phys. **51**, 4678 (1980).
[21] D. H. Kalantar, B. A. Remington, J. D. Colvin, K. O. Mikaelian, S. V. Weber, and L. G. Wiley, Phys. Plasmas **7**, 1999 (2000).
[22] K. T. Lorenz, M. J. Edwards, A. F. Jankowsky, S. M. Pollaine, R. F. Smith, and B. A. Remington, High Energy Density Phys. **2**, 113 (2006).
[23] S. M. Bakharakh, O. B. Drennov, N. P. Kovalev, A. I. Lebedev, E. E. Meshkov, A. L. Mikhailov, N. V. Neumerzhitsky, P. N. Nizovtsev, V. A. Rayevsky, G. P. Simonov, V. P. Solovyev, and I. G. Zhidov (unpublished).
[24] R. D. Richtmyer, Commun. Pure Appl. Math. **13**, 297 (1960).
[25] E. E. Meshkov, Izv. Akad. Nauk SSSR, Mekh. Zhidk. Gaza **4**, 151 (1969).
[26] J. G. Wouchuk, Phys. Rev. E **63**, 056303 (2001).
[27] K. O. Mikaelian, Phys. Fluids **17**, 034101 (2005).
[28] J. Walter, D. Yu, B. J. Plohr, J. Grove, and J. Glimm (unpublished).
[29] A. C. Robinson and J. W. Swegle, J. Appl. Phys. **66**, 2859 (1989).
[30] J. W. Swegle and A. C. Robinson, J. Appl. Phys. **66**, 2838 (1989).
[31] ABAQUS, Finite Element Code, Version 6.6 (Hibbit, Kalsson and Sorensen, Inc., Pawtucket, RI, 2006).
[32] A. R. Piriz, O. D. Cortazar, J. J. Lopez Cela, and N. A. Tahir, Am. J. Phys. **74**, 1095 (2006).
[33] K. O. Mikaelian, Phys. Rev. E **47**, 375 (1993).
[34] R. Hide, Proc. Cambridge Philos. Soc. **51**, 179 (1955).
[35] W. H. Ride, Proc. Cambridge Philos. Soc. **57**, 415 (1961).
[36] J. W. Miles (unpublished).
[37] G. N. White (unpublished).
[38] D. J. Steinberg, S. G. Cochran, and M. W. Guinan, J. Appl. Phys. **51**, 1498 (1980).
[39] J. Edwards, K. T. Lorenz, B. A. Remington, S. Pollaine, J. Colvin, D. Braun, B. F. Lasinski, D. Reisman, J. M. McNaney, J. A. Greenough, R. Wallace, H. Louis, and D. Kalantar, Phys. Rev. Lett. **92**, 075002 (2004).